

A Cryogenic Scan Mechanism for use in Fourier Transform Spectrometers

Claef F. Hakun* and Kenneth A. Blumenstock*

ABSTRACT

This paper describes the requirements, design, assembly and testing of the linear Scan Mechanism (SM) of the Composite Infrared Spectrometer (CIRS) Instrument. The mechanism consists of an over constrained flexible structure, an innovative moving magnet actuator, passive eddy current dampers, a Differential Eddy Current (DEC) sensor, Optical Limit Sensors (OLS), and a launch lock. Although all the components of the mechanism are discussed, the flexible structure and the magnetic components are the primary focus. Several problems encountered and solutions implemented during the development of the scan mechanism are also described.

INTRODUCTION

CIRS OVERVIEW

The CIRS is a remote sensing instrument designed for the Cassini spacecraft which will be launched in October 1997. The primary science objectives of the CIRS are:

- To globally map the thermal structure, gas composition, hazes and clouds, and non-equilibrium processes of Saturn and Titan.
- To search for new molecular species in the atmosphere of Saturn and Titan.
- To globally map the surface temperature of Titan.
- To map the thermal characteristics and composition of the rings and icy satellites.

The CIRS will provide the highest resolution interferograms of Saturn and associated targets to date. The top view of the Optical Assembly (OA) and the instrument coordinate system are shown in Figure-1. The instrument consists of the following sub-systems:

OPTICAL The optical system¹ consists of a Cassegrain telescope and three Michelson interferometers. The Mid-Infrared (MIR) and Far-Infrared (FIR) science interferometers provide for a spectral coverage from 7 to 1000 microns. The Reference interferometer (RI) provides signals used for instrument timing and data collection and control of the Scan Mechanism.

MECHANICAL The beryllium telescope assembly, 80K radiative cooler assembly, the relay optics and detectors, and scan mechanism are all mounted on the monolithic aluminum optical plate and constitute the OA. The OA is mounted to the spacecraft via a titanium mounting tube which provides pointing stability and thermal isolation. The scan mechanism is fastened and pinned to the OA on three coplanar mounting pads. The OA is designed to provide access to and alignment of all critical components.

ELECTRICAL The CIRS Electronics Assembly (CEA), is connected to the OA via a cryogenic cable which minimizes the thermal input between the warm CEA and the colder OA. The CEA controls all functions of the CIRS instrument: In particular the CEA contains the Scan Mechanism Electronics (SME). The SME performs the following

* Code 723, NASA Goddard Space Flight Center, Greenbelt, MD

major functions: phase-locked loop scan control, flyback control, engineering telemetry, unlatching control, and state selection of the mechanism. Describing the SME design constitutes the subject of another paper.

THERMAL The passive thermal design provides temperature stabilization at 80K for the MIR detectors and 170K for the rest of the OA. Heaters provide 0.1K per day stability of the 170K and 80K regions of the instrument. The main shaft of the SM must also meet this requirement.

MECHANISM Several mechanisms are utilized on the optical assembly; two cover release mechanisms, a calibration shutter mechanism² and the scan mechanism. The scan mechanism design, as with most instrument mechanisms, relates to all of the instrument subsystems.

FUNCTIONAL DESCRIPTION

The scan mechanism provides the optical alignment for the moving mirrors of the three interferometers. It provides precision linear translation of the retroreflector shared by the MIR/RI interferometers and the dihedral mirror for the FIR interferometer. The main shaft supports the retroreflector on one end and the dihedral on the other. Events are shown (Figure-2) which occur as the main shaft translates between its limits of travel. Motion of the main shaft modulates the incoming wavefronts of the interferometers to create interference between the fixed and moving arms. The data collected during a scan contains the amplitude and frequency content of the light collected by the field of view of the instrument. The scan mechanism has two main operational states; scan and flyback. When in the scan state, the mechanism translates in the -X direction. The main shaft velocity is precisely controlled by the phased-locked loop circuitry located in the SME. The mechanism continues to scan until given the flyback command from the Instrument Data System or until the end of scan OLS is triggered. Variable scan lengths are therefore possible. The majority of scans will either be short 0.4 mm scans or long 10.4 mm scans. The long scan is not centered on mechanism neutral (At the center of displacement where the spring forces are zero in the x axis). Skewing the long scan makes the average power dissipation equal for both long and short scans. In the flyback state, the mechanism translates in the +X direction at a rate approximately 20 times the nominal scan velocity. When the end flyback OLS is triggered, the mechanism begins scanning again. During the 4 year operational phase of the mission, the scan mechanism will continuously toggle between these two states.

HERITAGE

The CIRS is similar to the Infrared Interferometer Spectrometer (IRIS) instruments which flew on Voyager I and II. Similar mechanism concepts were implemented on each of these instruments, however, due to the stringent spacecraft limitations on mass and power, operating environment, and science requirements which provide for significantly broader spectral coverage and 10 times the resolution of previous missions, it is believed that the CIRS scan mechanism represents the state of the art design of a mechanism of this type.

MECHANISM OVERVIEW

The requirements, electromechanical design and operation, and testing of the scan mechanism are described. The scan mechanism design evolved over a two year period. Two developmental breadboard units were assembled and tested. Two engineering unit mechanisms which represent the flight design have been fabricated and tested. Two flight units are being assembled and tested.

REQUIREMENTS

The environmental and performance requirements listed below were developed at the Cassini Spacecraft³ and CIRS instrument⁴ levels directly from science requirements or engineering analyses. All testing and analysis of the engineering model scan mechanism indicate compliance with the following requirements.

SPACECRAFT LEVEL

- Survive the launch environment. Cassini will be launched on a modified Titan IV.
- Meet performance requirements while being subjected to spacecraft jitter disturbances. The reaction wheel disturbances represent the major disturbances during instrument operation. The effect of disturbances generated by other instruments will be minimized by scheduling observations and operation of other disturbance sources.
- All components to be insensitive 100Krad radiation environment
- Constitute < 2.5 nanotesla and < 10 nanotesla at 1 meter to instrument static and dynamic stray magnetic field budgets respectively. Meet AC stray magnetic field requirements.

INSTRUMENT LEVEL

- Contribute < 2.0 kg to instrument mass
- Fit into the OA and provide 160 mm metering distance between the vertex of the retroreflector and the apex line of the dihedral mirror. Allowable volume: X (134mm), Y (180mm), Z (165mm)
- Provide travel for variable length scans between 0.4 mm and 10.4 mm
- Dissipate an average of < 200 milliwatts @ 170K
- Operate for over 5 million fully reversing cycles over the 12 year mission
- Provide spring and actuator force constants which have < 5% deviation from linearity. This requirement was derived from analysis of the control system. Since all degradation effects are known, a minimum force margin of 50% is sufficient.
- Provide precision alignment and translation of the optical elements which have an allocated combined mass of 240 grams.
- Tilt of main shaft about the Y and Z axes to be < ± 3 arcseconds under zero g, at 170K and throughout the entire scan. Repeatability between scans < 0.15 arcsecond.
- Shear, defined as translation in the transverse Y and Z directions from nominal optical axis, to be < 6 microns under zero g, at 170K and throughout entire scan. Repeatability between scans < 0.5 microns.
- Allowable shear during ground testing to be < 18 microns throughout the entire scan.
- Provide a nominal scan velocity of 0.0208 cm/s.
- Provide for a minimum 69% scan efficiency for short scans and 95% for long scans.
- Control scan velocity to 5% (ZPD)/15% (elsewhere) rms in presence of disturbances.

ELECTROMECHANICAL DESIGN AND OPERATION

The top level assembly, each sub-assembly, and mechanism testing are summarized. The spring pair, actuator, outrigger/damper, launch lock, OLS, and compensation coil sub-assemblies form the top level assembly. The CIRS engineering model scan mechanism (Figure-3) cross-sectional view (Figure-4) depicts the major components of the scan mechanism top level assembly in the launch-locked configuration. The mechanism design has the following salient features:

- A flexible structure which supports the main shaft
- An innovative moving magnetic circuit with precision layer winding
- A Differential Eddy Current (DEC) sensor for analog displacement telemetry
- Passive electromagnetic dampers on both the main shaft and the outriggers
- Optical limit sensors (OLS) to provide end of travel indications
- Remotely resettable launch lock
- Compensation coil to minimize stray magnetic fields.

TOP LEVEL ASSEMBLY A spring pair assembly is attached to each end of the main shaft and to each end of the main housing. The outrigger shafts connect the spring pair assemblies. The main housing and the components referenced above constitute the flexible structure. The outrigger shafts pass through the outrigger dampers and are constrained only by the eddy current damping produced when the damping rings which are rigidly attached to each outrigger are translated through the radial magnetic field of the closed magnetic circuit of the dampers. The actuator magnetic circuit is contained between the two halves of the main shaft. The moving magnet configuration provides for minimal power dissipation on the main shaft and therefore minimal temperature increases of the main shaft occur during operation. Embedded within the main shaft is the bobbin assembly which is rigidly attached to the main housing. The bobbin assembly includes the DEC sensor windings, and the winding and single turn damping ring of the actuator. A tab is attached to the main shaft which triggers the OLS's directly after the end of long scan and at the end of flyback location. The launch lock constrains the mechanism whenever the mechanism is subjected to sizable vibration inputs. When unlatched, the main shaft is constrained by the tab of the launch lock and the endcap of the FIR spring pair assembly.

As the main shaft is displaced from mechanism neutral, the outriggers breathe in the radial direction and traverse half the displacement of the main shaft. This allows the springs to deform in almost pure bending. The mechanism can be viewed as three double four-bar-linkages each in parallel. In Figure-4, one of double four-bar-linkages is clearly visible. The load path goes from the inner springs which are rigidly attached to the main housing up to the outriggers and then down the outer springs which connect to the main shaft. A quick and fairly accurate method to calculate the axial stiffness of a mechanism of this type is to make an imaginary cut of one of the springs at the midpoint and impose a displacement condition. The flexible structure of the mechanism can now be reduced to a system of cantilever beams in series and in parallel with each other. The main housing, outriggers, and main shaft constitute the metering structure of the mechanism and are made of aluminum 6061 to match the OA. This ensures that gross misalignments between optical elements due to CTE mismatches does not occur.

This configuration results in a mechanism which has an extremely linear axial force versus displacement relationship, relatively high radial stiffness, minimal power dissipation on the main shaft, thermal stability and precision mirror positioning capability.

SUB-ASSEMBLIES

Spring Pair Assembly The spring pairs provide the support, alignment and guidance of the main shaft and outriggers. The spring pair assembly pictured in Figure-5 is the result of a precision matched machining and pinning assembly procedure. The assembly procedure ensures that the spring clamping surfaces are flat and coplanar to within 5 microns and that the spring lengths are all equivalent to within 5 microns. The assembly is fastened to the main housing, outrigger/damper assembly, and the actuator assembly. The design of the spring pairs allows for repeatable assembly into the top level assembly of the mechanism without the need to perform complicated and time consuming realignment procedures. The performance of the design is relatively insensitive to preloading of the clamping surfaces and is therefore insensitive to changes in bulk temperature of the components.

The assembly consists of 6 beryllium copper leaf springs, and the following AL 6061 T651 structural components: the endcap, outrigger components, clamp plates, and the mirror mount hub. The endcap and mirror mount hub are thermally cycled to ensure stability at 170K. All aluminum parts are black anodized. Fixture heat treating of the beryllium copper to the TH02 (half hard) condition enhances the physical properties, relieves residual stresses and flattens the springs. In the TH02 condition, beryllium copper has excellent fatigue and strength properties, relatively good thermal conductance, and good stability of the elastic modulus over the operating temperature range. The springs are 0.3 mm (0.010") thick, 28 mm (1.1") wide and 68mm (2.670") long. These dimensions provide the desired force constant (600 N/m), fatigue life (infinite: 10.5 ksi maximum bending stress), and radial stiffness.

Actuator Assembly The actuator assembly (Figure-6) provides mechanical force required to overcome the axial spring force and required to control displacement and velocity of the main shaft. It incorporates passive eddy current damping and position monitoring of the main shaft. This assembly is composed of three primary sub-assemblies; the moving magnetic circuit, the fixed bobbin, and DEC sensor assemblies.

Magnetic Circuit The moving magnetic circuit is divided into two symmetric halves. Each half consists of the inner housing, pole piece assembly, and axial magnet. The pole piece assembly is epoxy bonded with Stycast 2850/24LV and consists of the pole piece, sectioned radial magnet and a thin Carpenter 430F solenoid quality stainless magnet containment ring. The inner housings and pole pieces, machined from Hiperco 50a, provide a low reluctance magnetic path which completely encloses the air gap of the actuator and carries the flux of the SmCo 28 magnets. The magnetization directions of the axial and radial magnets are indicated in Figure-6. The magnets and Hiperco 50a components are sized to provide a maximum flux of 2 tesla within the magnetic circuit. This configuration results in the extremely linear current versus displacement relationship (Figure-9).

Bobbin The bobbin supports the DEC sensor, the actuator winding, and the main shaft damping ring. The bobbin is made of 6061-T651 aluminum which is black anodized to ensure non-conduction between the winding and the bobbin structure. The bobbin is rigidly attached to both endcaps by six integral legs which pass axially through holes in the inner housings and radial magnets. Grooves have been machined on each of the legs on one side of the bobbin to provide a path for the six wires which exit the actuator assembly. Two wires are carried on each leg. In addition, the bobbin has 61 parallel circular grooves precisely machined and located between the side walls of the bobbin. These grooves mimic a perfect layer of the winding. This precision layer winding has exactly 24 layers and 61 turns per layer of 32AWG magnet wire. The cross-section photograph (Figure-6) reveals its uniformity. The winding is encapsulated with Stycast 2850/24LV according to a vacuum/high pressure impregnation procedure which assures that no voids are present within the winding. The encapsulant is also used to secure the high purity copper damping ring which slides over the outer diameter of the bobbin. Passive eddy current damping of the main shaft works on the same principle as that of the outrigger dampers. The winding produced by this process is highly reliable, easy to wind, and approaches maximum achievable fill factor of copper within the air gap and therefore maximum actuator efficiency.

Differential Eddy Current (DEC) Sensor The DEC sensor provides an analog voltage output proportional to displacement of the main shaft. The sensor consists of excitation and pick-up windings which are coupled by two aluminum tubes which are integral to the main shaft halves. Windings are centrally located within the main shaft. The sensor operates differentially; one tube couples as the other decouples when the main shaft is displaced from mechanism neutral. The coupling between the excitation and pick-up coil induced by a 20 kHz excitation signal is demodulated and filtered with a standard LVDT signal conditioning chip to provide the analog output of the sensor. Linearity and resolution of the sensor is shown in Figure-10.

Actuator Parameters

Actuator constant (Ka), 170K	5.0 N/√W	Actuator constant (Ka), 293K	3.6 N/√W
Force constant (Kf)	30.1 N/A	Damping	17 N/m/s
Diameter (w/o shaft)	40.6 mm	Length	63.5 mm
Moving mass	272 g	Mass, fixed (w/o sensor)	74 g

Outrigger/Damper Assembly A single turn high purity copper damping ring is rigidly attached to the outrigger shaft and is in the air gap of the magnetic circuit (Figure-7). The magnetic circuit consists of a single SmCo 28 radial magnet and a closed Hiperco 50a low reluctance magnetic path. The circuit is designed to carry a maximum flux of 2 tesla. As the damping ring is translated through the radial magnetic field, eddy currents are generated. These currents create a force which is proportional to the velocity and in opposition to the direction of motion of the ring. The value of damping was determined by the control system model, the allowable volume, and the spring dimensions. The dampers are sized to provide critical damping at the resonance of the outriggers when located at the mechanism neutral position. The damping increases by a factor of ~ 1.9 at 170K due to decrease of resistance of the damping ring.

Launch Lock Assembly The housing, guide shafts, and yoke comprise the structure of the launch lock (Figure-8). Return springs located on both guide shafts provide the force required to reset the High Output Paraffin (HOP) actuator and maintain the yoke in the latched configuration during launch. Optical limit sensors are triggered when the yoke is displaced ~ 1.3 mm (0.05") from either end of travel of the yoke within the housing. The first OLS provides an indication that the yoke is in the proper unpowered location. The second OLS ensures that power is removed from the HOP prior to the yoke being driven into the hard stop which could damage the HOP.

In the locked configuration, the main shaft is displaced to the MIR end of travel and constrained in the axial direction by interaction of tabs located on the yoke and main shaft and by radial stops on the main housing (Figure-4). Motion of the outriggers is limited by snubbers. To unlatch, power is applied to the HOP actuator. The drive shaft of the HOP overcomes the 17.8 to 44.5 N (4 to 10 lb) return spring force and displaces the yoke ~ 12.7 mm (0.5") in the Y direction. This disengages the yoke and main shaft tabs. Once disengaged, the main shaft is forced to the mechanism neutral position by the flexible structure of the mechanism. After the second OLS is triggered and power is removed from the HOP, the yoke returns to its original unpowered position. The yoke tab now becomes the hardstop in the +X direction. To relatch, power is applied to the HOP driving the yoke in the +Y direction. The main shaft is then commanded to the MIR hardstop. Power is removed from the HOP and the yoke returns to the unpowered position, thus constraining the main shaft in the axial direction. The lock is therefore remotely resettable.

OLS Assembly The OLS's provide precision displacement information of the main shaft and the launch lock yoke (Figure-8). Each sensor consists of an LED and phototransistor pair secured by urethane in aluminum housings. Half of the aperture of the phototransistor is obscured by an aluminum structure. When the blocking tab crosses the aluminum edge, no light impinges on the detector. A relatively sharp transition occurs. Resolution is measured to be $\ll 3$ microns. This design utilizes the stability of the aluminum edge and a threshold circuit to determine the transition point. The OLS's are insensitive to relative motion between the LED and the phototransistor and to changes in their optoelectronic behavior after exposure to radiation.

Compensation Coil Assembly The compensation coil assembly (Figure-4) when energized counteracts the residual dynamic stray magnetic field of the scan mechanism. It consists of 25 turns of 26 gage lead wire. The coil polarity is such that as the drive current increases, the magnetic field of the compensation coil increases with an opposing field.

MECHANISM TESTING The engineering model scan mechanism has been extensively tested at the component, SM/RI subsystem, and OA levels to ensure compliance with requirements. Component level testing includes verification of mechanism parameters and performance. The axial spring and actuator constants, tilt, shear, and sensor outputs are some of the parameters which are measured at both ambient and 170K. Stray magnetic field and launch vibration testing occurs at this level. The SM and RI are also tested as a subsystem prior to integration into the OA. A dewar with optical quality windows was designed for both component and sub-system testing. Jitter sensitivity

testing is performed at the SM/RI subsystem level. System-level performance and environmental testing is also conducted during OA level testing.

PROBLEMS/SOLUTIONS

How should a mechanism be designed so that it can be repeatably assembled and disassembled and yield consistent performance characteristics? How can some of the inherent non-linearities of this type of mechanism be overcome? How could a linear actuator with permanent magnets be designed to radiate extremely low stray magnetic fields? These are just a few of the questions which required answers during the development of the CIRS scan mechanism. A description of these problems and how they were solved is now provided.

ASSEMBLY PROCESS

Since the flexible structure overconstrains the main shaft, it is important that care be taken to equalize the length of each spring to ensure that a snap through buckling behavior of the springs does not occur. Excessive buckling will cause increased non-linearity about the mechanism neutral position. The length of the main shaft and the three outriggers are critical to the tilt and snap performance of the mechanism as the main shaft is displaced from mechanism neutral. Spacers have been designed into the mechanism at both ends of the three outriggers and the main shaft to allow tuning of mechanism tilt and elimination of any snap through buckling behavior. The spring pair assembly procedure, careful measurement of all critical component dimensions, and lapping the adjustment spacers, the main housing, and outrigger interface surfaces ensure that the final assembly of the mechanism meets performance requirements. Measurements of current versus displacement and tilt versus displacement are made during the assembly process. Tilt sensitivity about the Y and Z axes versus displacement is shown in Figure-11. To illustrate the tilt sensitivity, a 200 gram unbalanced load was applied to the shaft during the measurement. Maximum tilt values of 2 to 3 arcseconds throughout the entire scan are readily achievable when the masses attached to each end of the main shaft are approximately equal. The actual masses of the optical elements are within 40 grams of each other. Acceptable tilt performance is a good figure of merit that the mechanism is assembled properly.

NONLINEAR CHARACTERISTICS

Although some aspects of scan mechanism performance indicated superior linearity in the axial direction, non-linear behavior related to translation of the main shaft in the axial direction is observed. Two major non-linearities inherent in the design which directly effect conformance to mechanism performance requirements are the changing radial stiffness and a shifting outrigger resonance.

RADIAL STIFFNESS VERSUS DISPLACEMENT The transverse stiffness of the flexible structure decreases as the main shaft is displaced from the neutral position of the mechanism. The structure is stiffest when all the springs are parallel to each other. The mechanism is said to shear under the influence of gravity. Shear of the main shaft under the influence of gravity as a function of displacement and increased loading of the main shaft is shown in Figure-12. Shear in the lateral direction to gravity does not deviate by more than 2 microns. The linear analysis conducted to design the original

developmental unit failed to accurately predict shear. After initial testing revealed unexceptionable shear performance, an extensive mechanism parametric analysis was conducted. The major parameters involved were moving mass, power dissipation, mechanism volume, outrigger damping, radial and axial stiffness, and fatigue stress. The development unit was modified and the performance of the new spring design was verified. Early "breadboarding" of designs even when some heritage of a particular design exists is critical to successful delivery of a mechanism.

SHIFTING OUTRIGGER RESONANCE Another non-linearity inherent in a design of this type is that as radial stiffness decreases, the fundamental resonant frequency of the outriggers increases as a function of the displacement of the main shaft. The mechanism has a shifting resonance. Indicated in Figure-13 is the frequency response of the mechanism with increasing offsets of the main shaft from the neutral point. The outrigger resonance shifts from ~ 25 Hz at the neutral point to ~ 90 Hz near the end of travel. This is highly undesirable from a mechanism control point of view. The response of the mechanism to external disturbances is highly dependent on the resonant frequency of the outrigger. External vibrations are amplified and mechanism velocity variation performance can suffer when the frequency content of the external disturbances coincide with the resonance of the outriggers. As in previous mechanisms of this type, outrigger dampers were designed to reduce the effect of outrigger resonances and enhance control of the mechanism. The subject of jitter sensitivity continues to be a concern. The control of the mechanism operating in a "quiet" environment as achieved velocity variation of less than 0.5%. The transmissibility and quantification of disturbances through the spacecraft and instrument structures has been the subject of extensive analysis and testing. In addition to the subsystem SM/RI jitter testing, spacecraft level testing is scheduled.

ACTUATOR DEVELOPMENT

From the beginning of this project, there has always been a great deal of concern about meeting stringent magnetic field requirements without compromising performance. It was decided to first consult with commercial vendors of linear actuators to gain expertise to select the most promising configuration. Otherwise, all work was done in-house. Software was written to perform parametric studies so as to optimize all the actuator parameters. Magnetic field modeling was performed to predict performance and stray magnetic fields and to explore various approaches to minimizing stray fields. A major emphasis was placed on designing the actuator to have minimal stray magnetic field.

CONFIGURATION A study was performed by Northern Magnetics⁵ to determine the optimal configuration for the actuator. A number of configurations were studied. A moving magnet type design was selected so that the heat generated by the winding could be easily sunk without the necessity for flexing thermal straps or power leads. A voice coil type design (no soft magnetic material associated with the coil) was selected to prevent radial actuator attractions. The selected configuration was expected to radiate minimal stray magnetic fields because the air-gap is nearly fully enclosed and the path for magnetic flux generated by the winding sees the high reluctance of the magnets, thus preventing excessive flux densities. Also, having the magnet material located away from the air-gap allows the flux to distribute very uniformly across the air-

gap (Figure-14) enhancing force constant linearity throughout the actuator displacement. The outrigger damper which has a radial magnet supplying magnetic flux directly across the air gap does not distribute flux as uniformly (Figure-14). This configuration is simple and adequate for the purpose of damping. However, if the actuator was designed to have a flux distribution like that of the damper, linearity would be degraded.

OPTIMIZATION An Excel spreadsheet program was written such that dimensional and material property parameters, force constant, and the force environment could be inputted. The output parameters are actuator constant, power, turns, wire size, resistance, current, force margin, damping, mass, etc. Using the Solver, an input value could be found to satisfy a desired output value. The program was used to examine the relationship between mass and power and look at other tradeoffs so as to best meet the requirements.

MAGNETIC FIELD MODEL A 2-D radially symmetric Boundary Element Model (BEM) was created using MAGNETO. With this model, better values for flux densities and actuator performance can be predicted. The BEM model can solve the flux distributions taking into account non-linear characteristics of the materials. Flux levels were of interest in the air gap (Figure-14) to predict force constant linearity and damping levels, in the soft magnetic material to minimize saturation which results in magnetic field leakage, in the magnets to see if operation was near the maximum energy product (BH) for minimum magnet volume. The BEM model was also used predict the magnetic field at 1 meter, but with questionable confidence due to the fact that those values are on the order of 10^8 smaller than the flux in the gap (Predicted values: 1.2 nT unpowered, 4.4 nT powered).

MAGNETIC FIELD IMPROVEMENT Magnetic field mapping was performed at the Spacecraft Magnetic Test Facility at GSFC using fluxgate magnetometers with the Earth's field canceled. The field shape resembles that of a dipole. A static (0 Hz, unpowered) level of 7 nanotesla (static spec: 2.5 nT @ 1 m for mechanism, 5 nT for instrument) was measured at 1 meter along the scan axis. However, powering so as to cause a full displacement results in a change in field of 23 nanotesla peak to peak (dynamic spec 10 nT p-p <10 Hz @ 1 m). The specifications were re-evaluated and it was determined that it would be beneficial reduce the level of dynamic magnetic field because of its effect on the Vector-Helium magnetometer on the spacecraft. A coil with 18 turns around the entire mechanism was connected in series with the actuator winding. Measurements showed that the dynamic magnetic field was reduced to 4 nT p-p. Due to dimensional constraints, the implemented compensation coil is smaller in diameter requiring more turns and is located asymmetrically.

CONCLUSION

The CIRS scan mechanism has achieved high precision linear motion for greater scan displacements than previously accomplished, necessary for high resolution infrared spectrometry. A uniquely designed moving magnet actuator with an integral coaxially located displacement sensor is incorporated into the scan mechanism. This actuator has high linearity, allows for temperature stability of the optical elements, and exhibits extremely low levels of stray magnetic fields. The actuator, dampers, and spring characteristics have been optimized and tailored to allow for superior controller performance so as to scan at very low velocities with minimal velocity variation. The CIRS scan mechanism is the result of extensive mechanical, optical, electromagnetic, and control system analysis and testing, consultation with fabrication and material experts, and the dedication of numerous hard working individuals.

ACKNOWLEDGMENTS

Gary Brown, Leonard Brown, Jason Budinoff, Mike Hagopian, Paul Haney, Susan Hill, Pat Humphrey, Sid Johnson, Chiachung Lee, Ken Lee, Jeff Mahmot, Billy Mamakos, Guy Michel, Armando Morell, Israel Moya, Dave Pfenning, Dwight Roberts, Jim Wall, Dot Wells, Wahid Zewari

REFERENCES

1. P. Maymon, M. Dittman, B. Pasquale, D. Jennings, K. Mehalick, C. Trout, "Optical Design of the Composite Infrared Spectrometer (CIRS) for the Cassini Mission." SPIE Vol 1945, (1993), Pg 100-110.
2. A. Tyler, "Shutter Mechanism for Calibration of the Cryogenic Diffused Infrared Background Experiment (DIRBE) Instrument." 20th Aerospace Mechanisms Symposium, (1986), Pg 97-102.
3. NASA/JPL, "Cassini Orbiter Functional Requirements Book Environmental Design Requirements." Rev A, CAS-3-240 (Insert to 699-205 Cassini Orbiter Functional Requirement Book), (11 February 1994).
4. NASA/GSFC, "Cassini/Composite Infrared Spectrometer Performance Requirements Document." CIRS-704-001 Rev B, (21 November 1994).
5. W. Hinds, M. Wilson, "Optimum Non-commutated DC Linear Motor." Northern Magnetics Technical Report N-101, (7 February 1992).
6. Munch et al., "Inductive Coupling Position Sensor Method And Apparatus Having Primary and Secondary Windings Parallel To Each Other." 5,036,275, (1991).

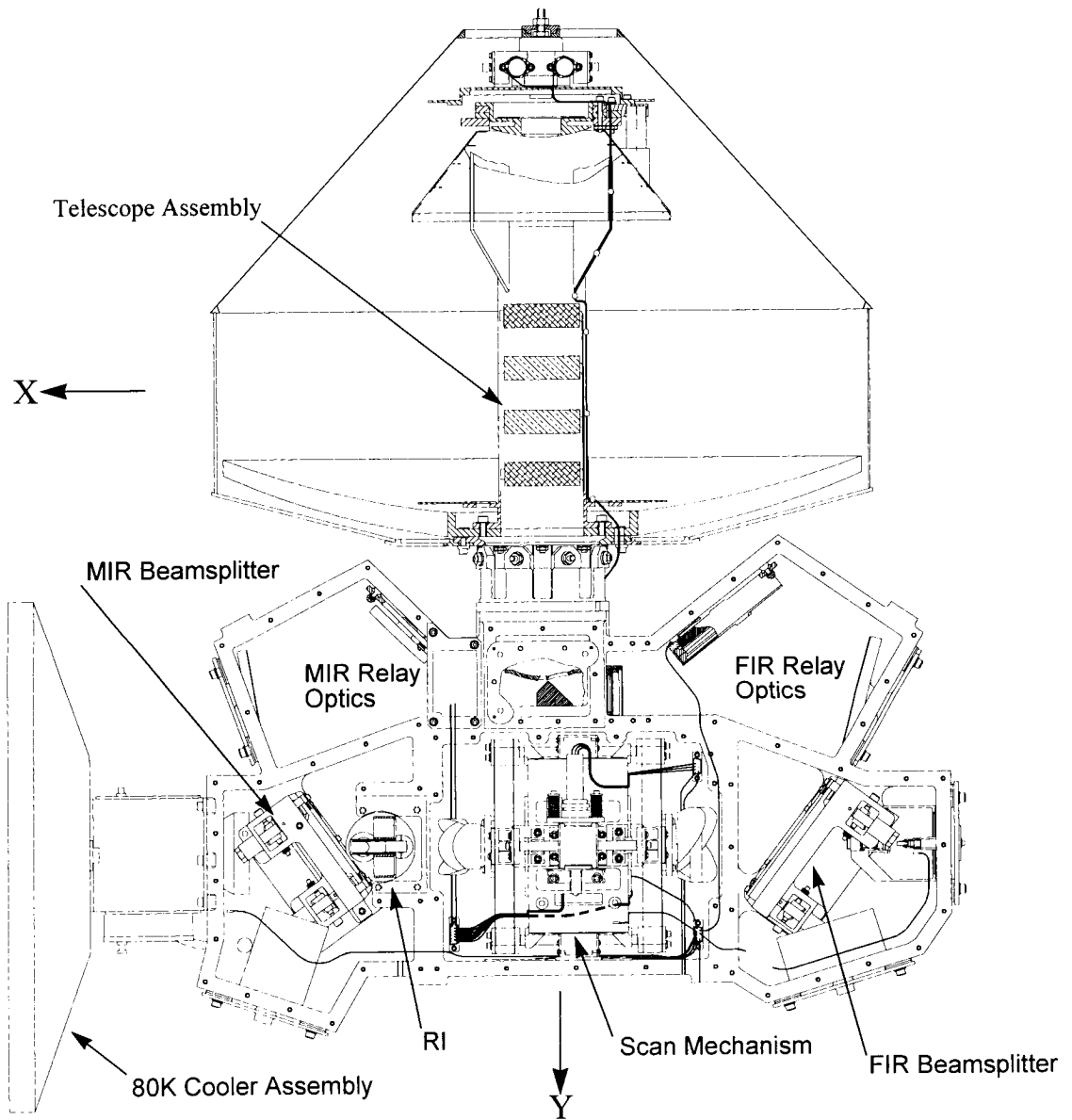
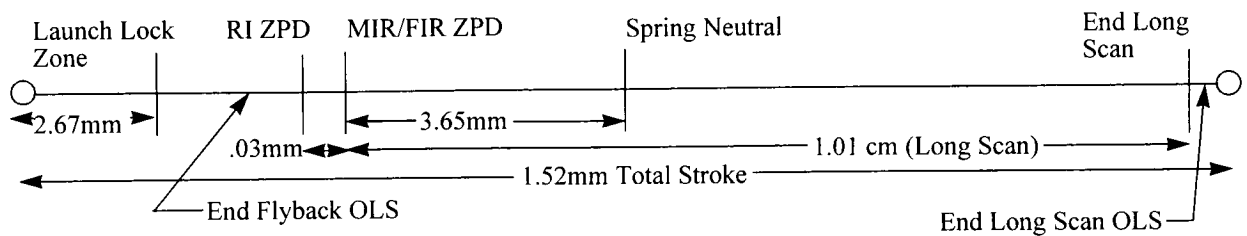


Figure-1 CIRS Optical Assembly



Zero Path Difference (ZPD)

Figure-2 Scan Mechanism Displacement

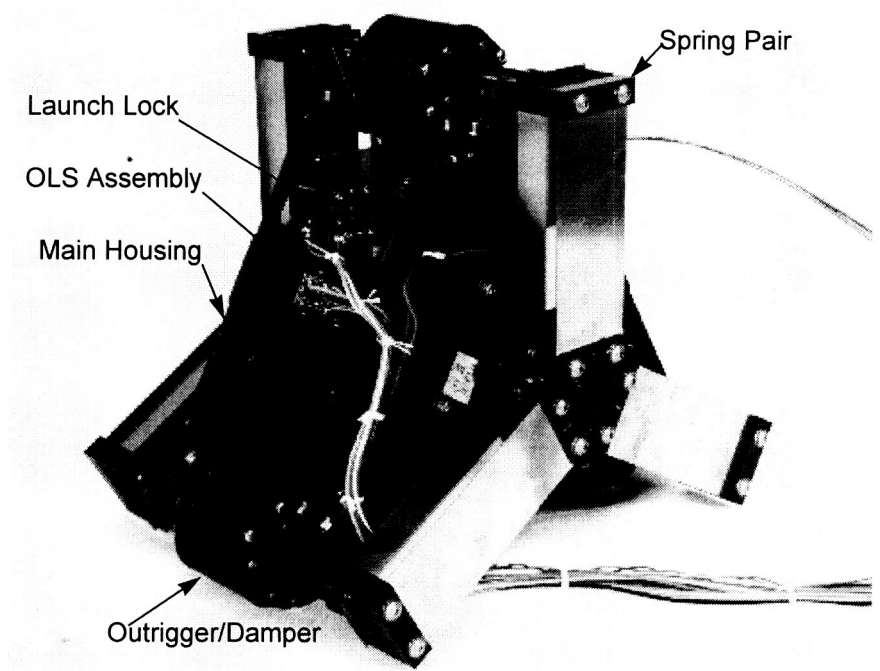


Figure-3 Engineering Model Scan Mechanism

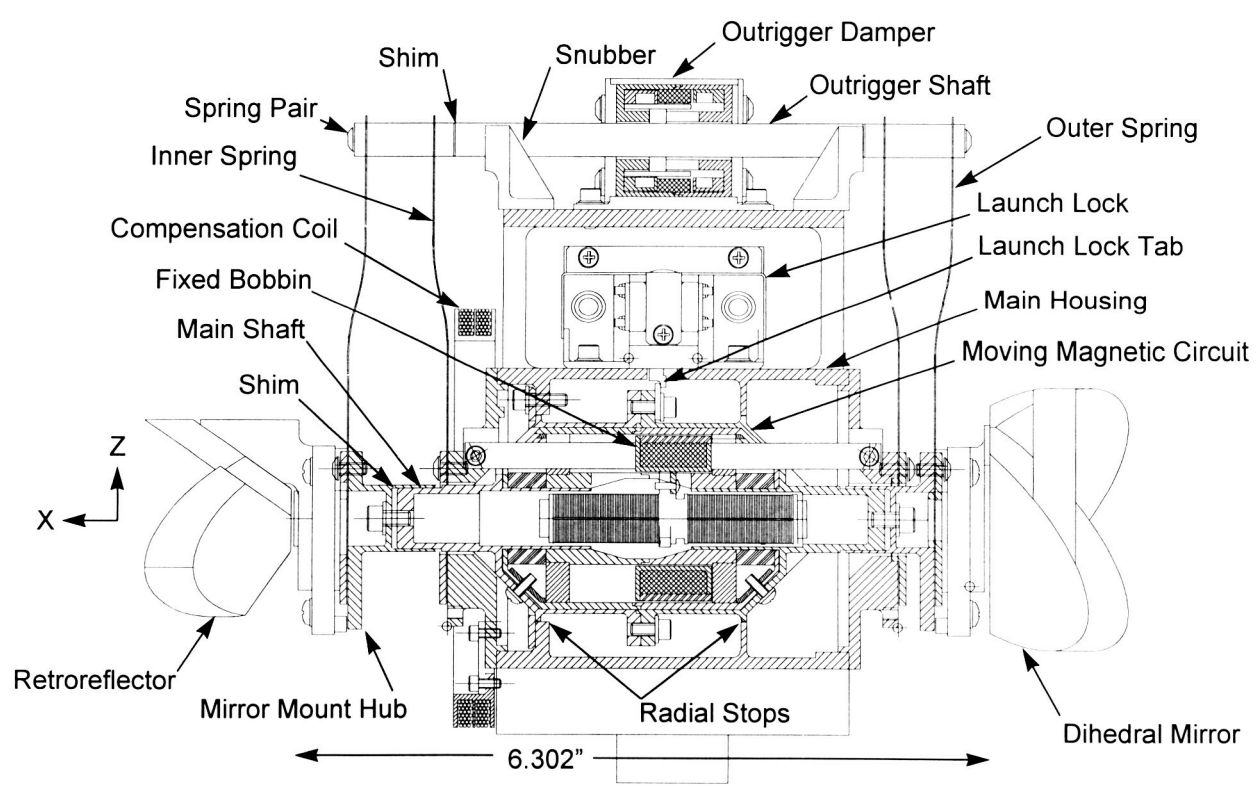


Figure-4 Scan Mechanism In Locked Configuration

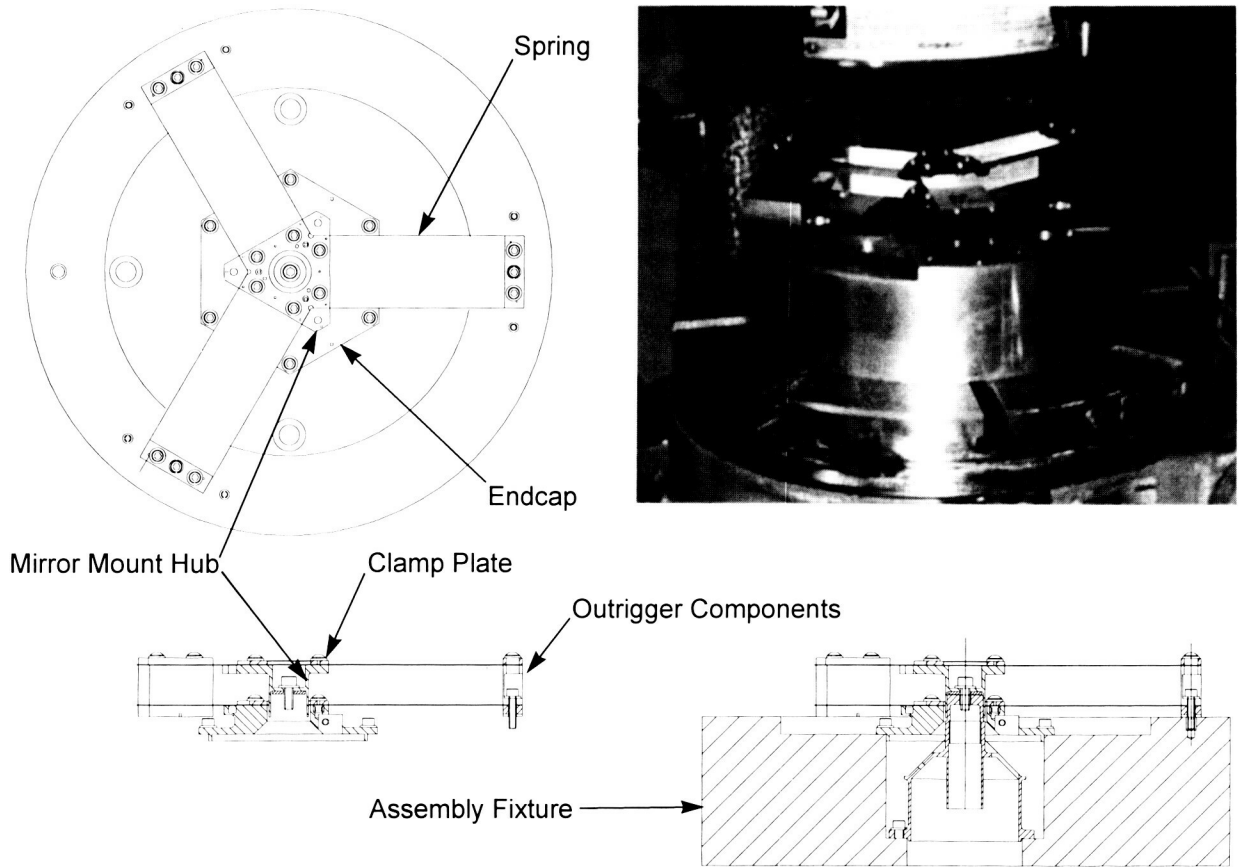


Figure-5 Spring Pair Assembly

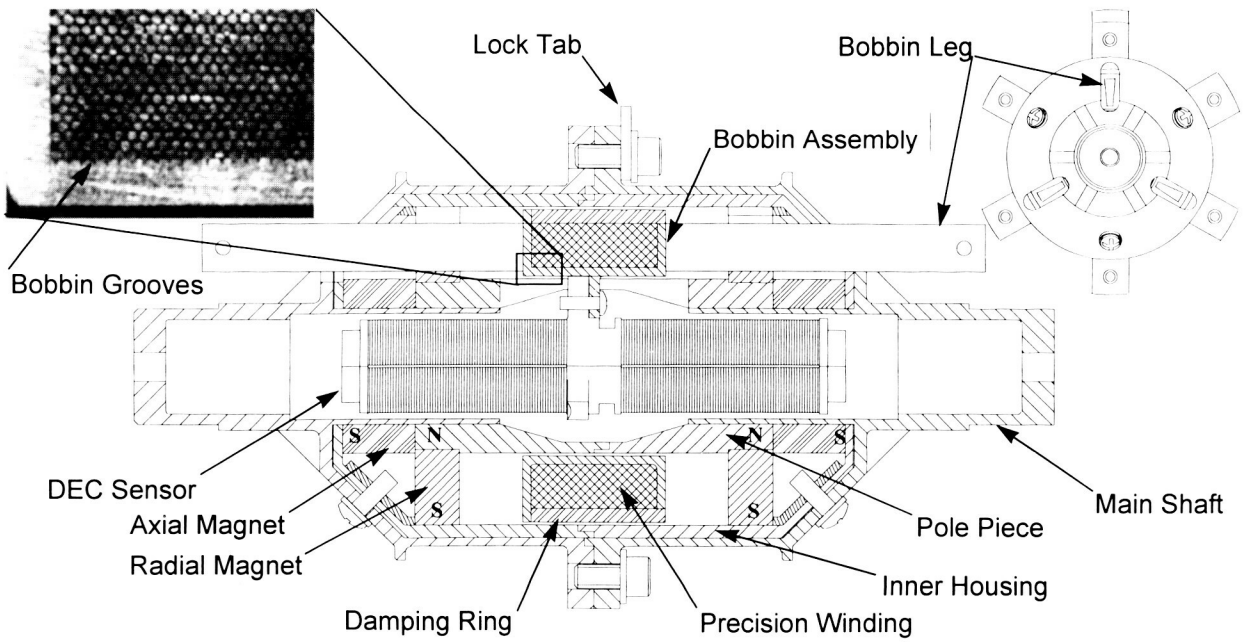


Figure-6 Actuator Assembly

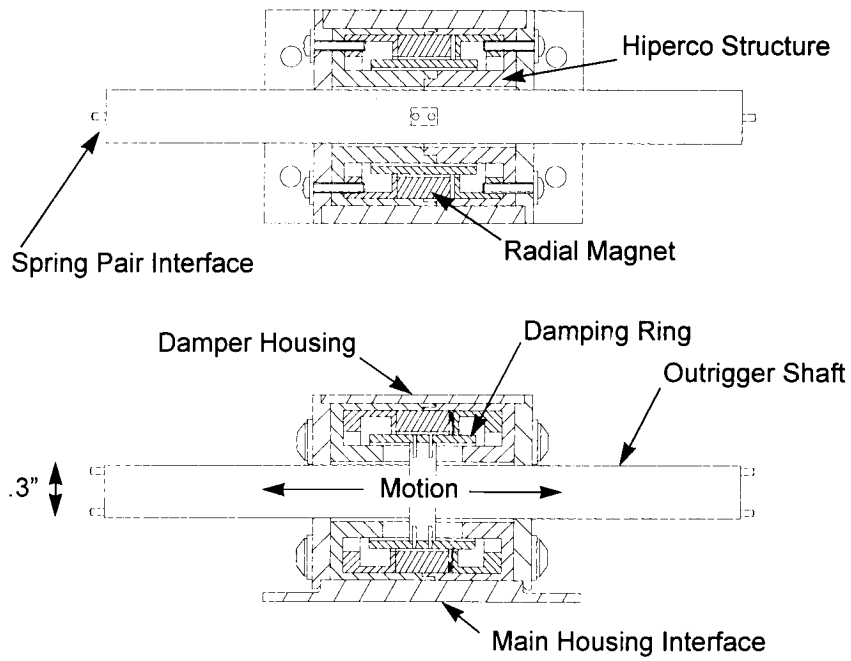


Figure-7 Outrigger/Damper Assembly

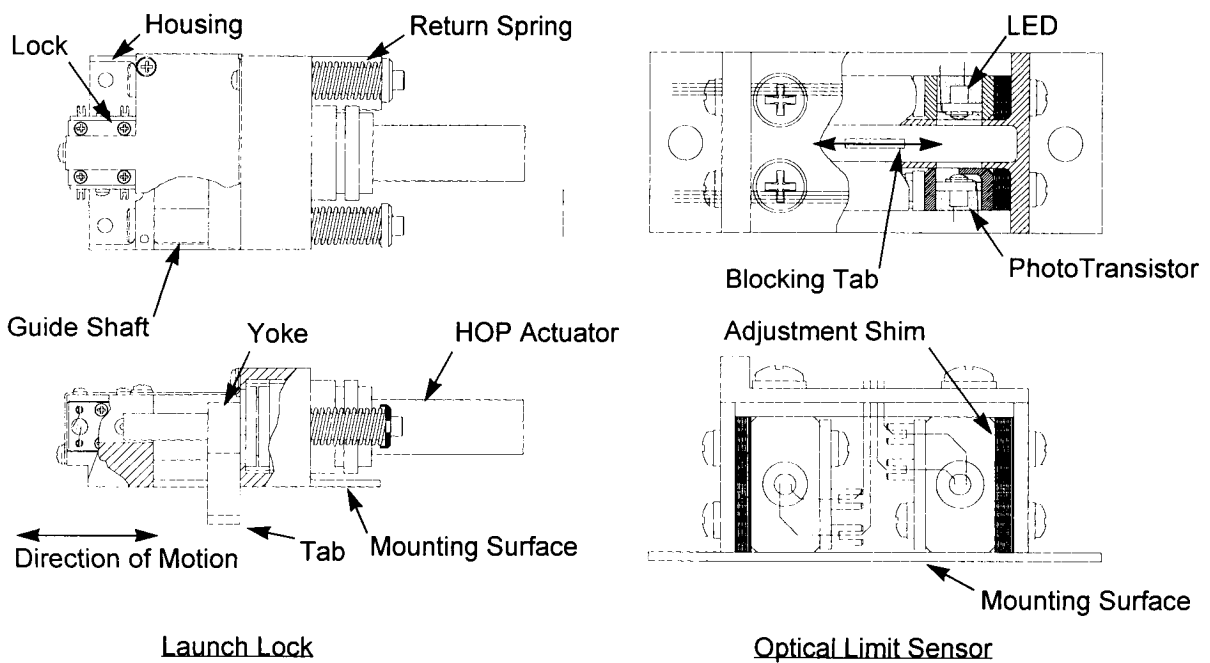


Figure-8 Launch Lock and Optical Limit Sensor Assemblies

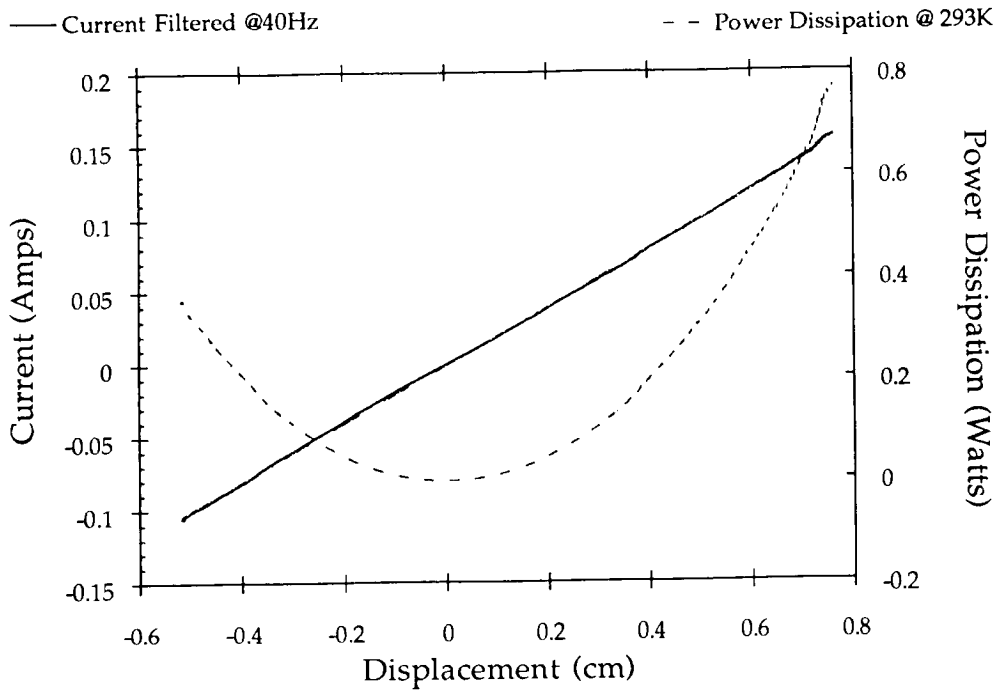


Figure-9 Current and Power versus Displacement

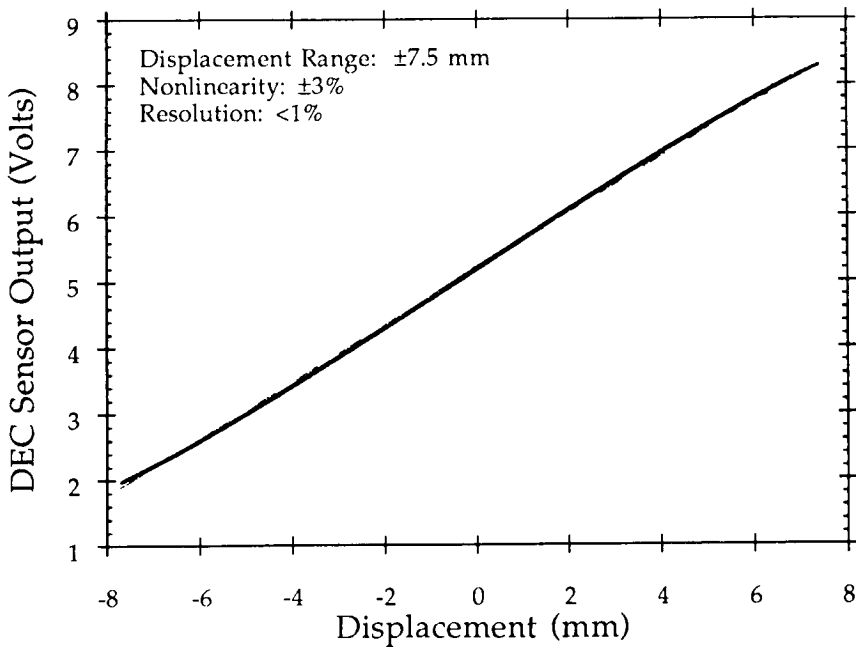


Figure-10 DEC Sensor Output versus Displacement

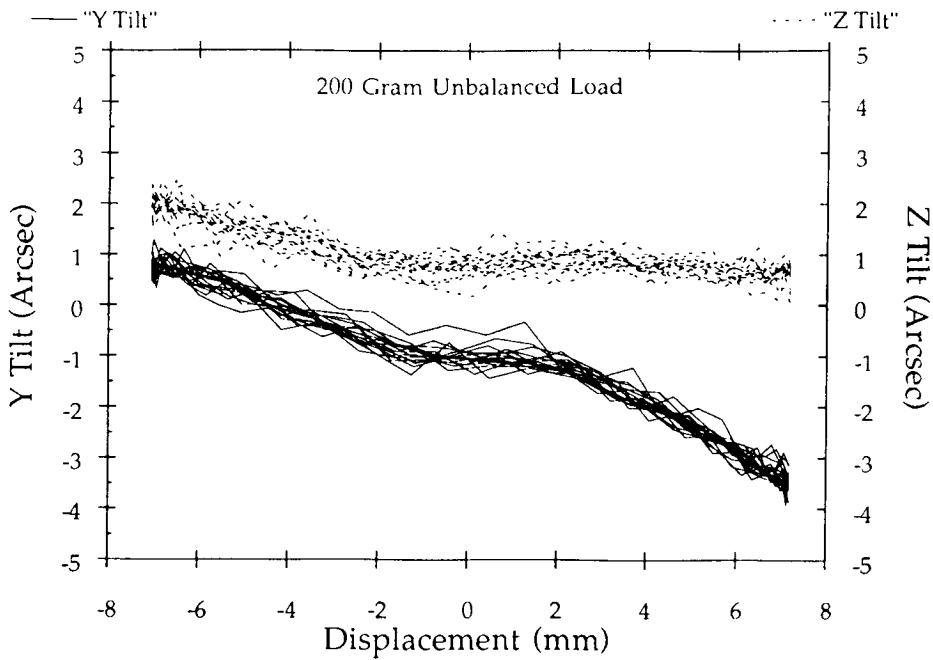


Figure-11 Y and Z Tilt versus Displacement

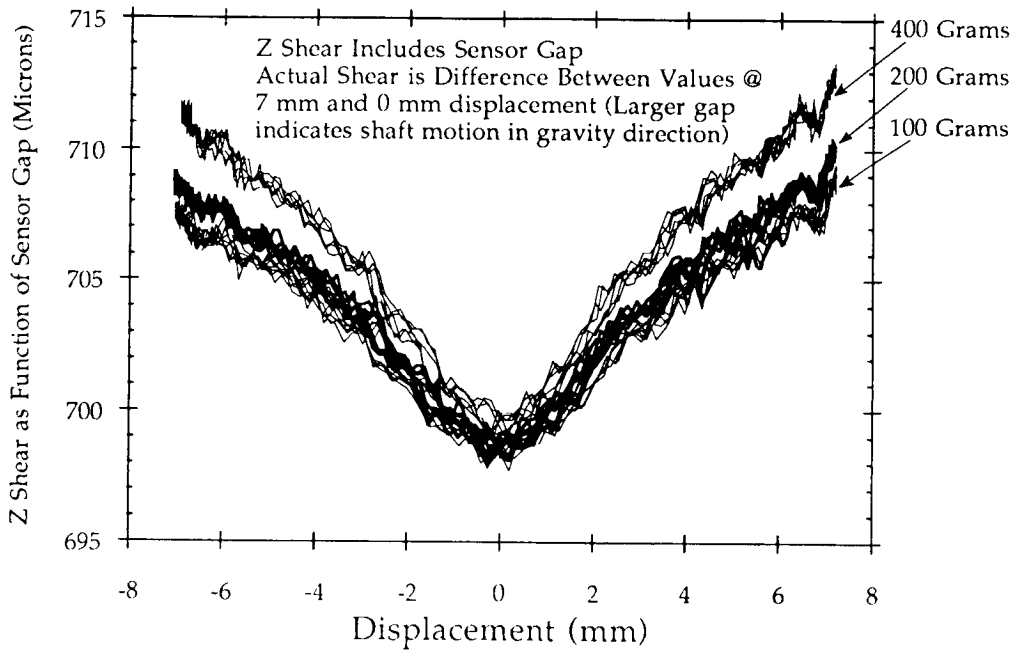


Figure-12 Shear Due To Gravity versus Displacement

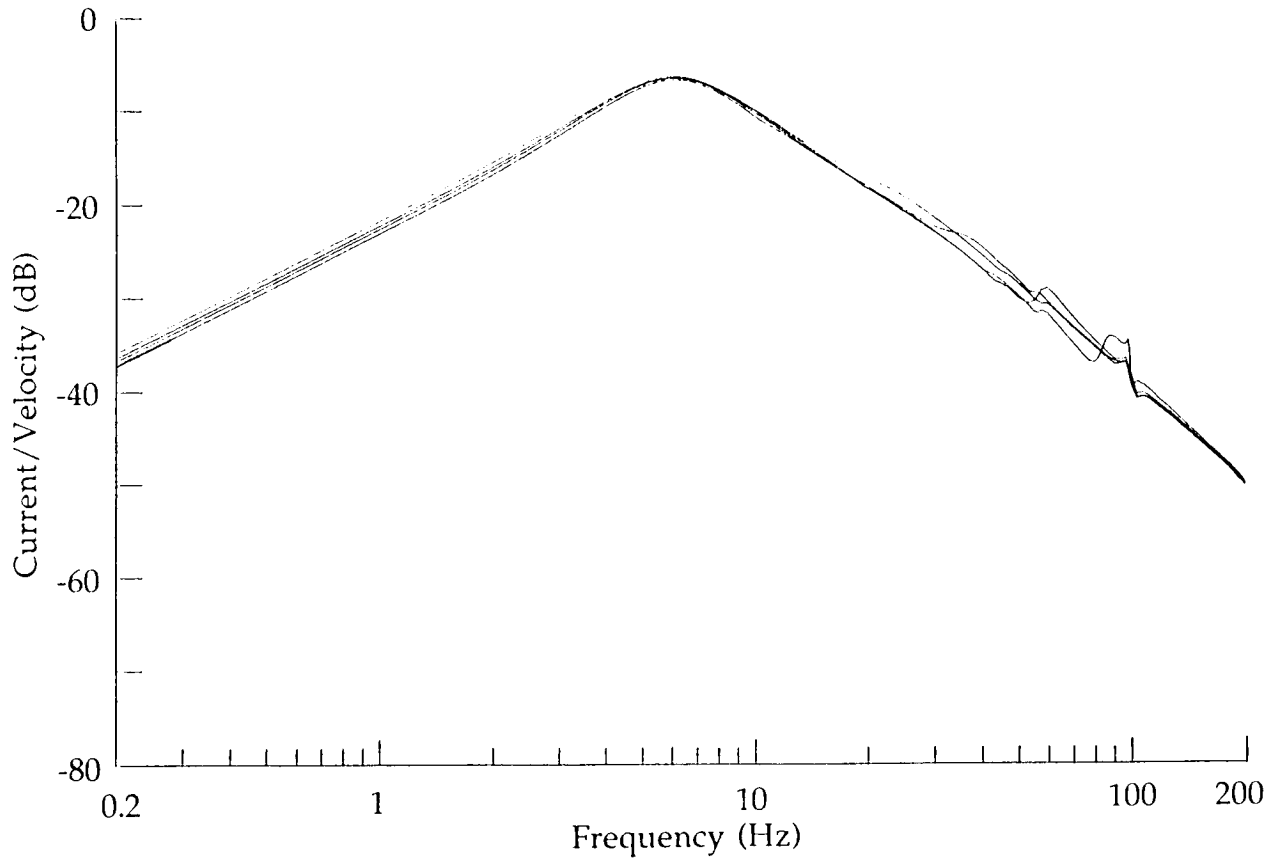


Figure-13 Mechanism Frequency Response

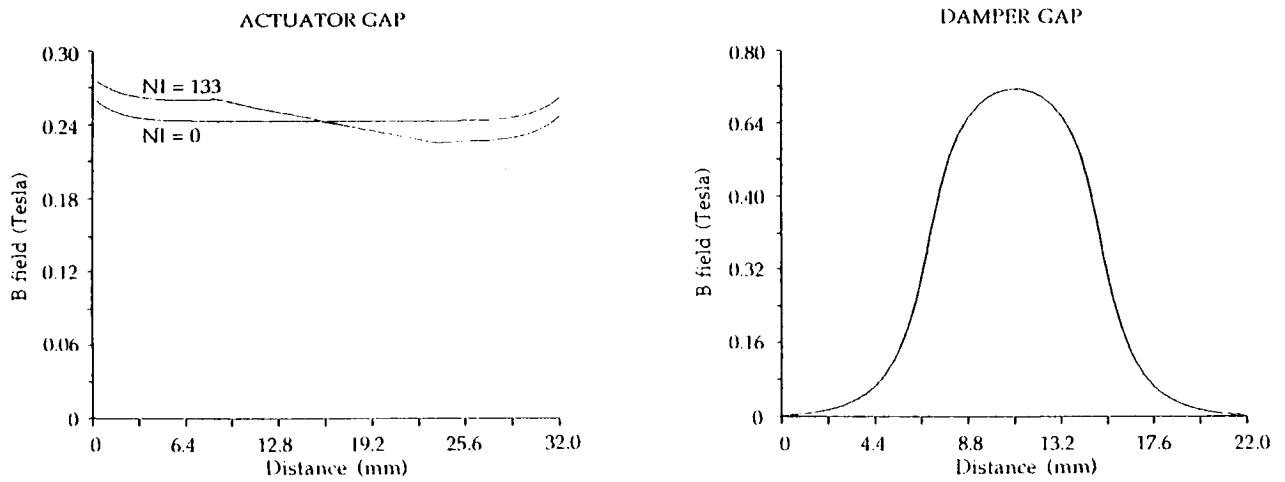


Figure-14 Magnetic Flux Models